Effect of deuteration in fluorescence- and phosphorescence-resolved optically detected magnetic resonance of metal-free dual singlet-triplet emitting OLEDs

F. Braun,[1] V. V. Mkhitaryan,[1] S. Bange,[1] M. Pauls,[2] S. Höger,[3] C. Bannwarth,[2] and J. M. Lupton[1]

[1]*Institut für Experimentelle und Angewandte Physik and Halle-Berlin-Regensburg Cluster of Excellence CCE, Universität Regensburg, Universitätsstraße 31, 93053 Regensburg, Germany*

[2]*Institut für Physikalische Chemie, RWTH Aachen, Melatener Straße 20, 52074 Aachen, Germany*

[3]*Kekulé-Institut für Organische Chemie und Biochemie, University of Bonn, Gerhard-Domagk-Straße 1, 53121 Bonn, Germany*

(Received 26 August 2026; accepted 26 October 2026; published 17 November 2026)

Dual singlet-triplet-emitting organic light-emitting diodes (OLEDs) based on metal-free room-temperature phosphorescence (RTP) materials offer unique opportunities to study electronic and nuclear spin dynamics. We investigate the influence of nuclear hyperfine fields, i.e., deuteration, on spin-dependent exciton formation in simple guest:host OLEDs based on the RTP compound 11,12-dimethyldibenzo[*a,c*]phenazine (DMDB) embedded in a 4,4′-bis(N-carbazolyl)-1,1′-biphenyl (CBP) matrix by using fluorescence- and phosphorescence-resolved optically detected magnetic resonance (ODMR). The ODMR response is governed by the interplay of the polaron-pair (PP) mechanism, where electronic spin precession in hyperfine fields controls exciton generation, and the triplet-exciton polaron (TEP) interaction, which mediates spin-dependent quenching of triplet excitons by polarons and hence phosphorescence. By combining phase-sensitive lock-in detection with a density-matrix-based description of the spin dynamics, we succeed in disentangling the strongly convoluted resonance line shapes arising from the superposition of the two processes. Simultaneous analysis of in-phase and quadrature lock-in signals yields consistent hyperfine-field strengths and electron-hole and exciton recombination rates. In contrast to pure hydrocarbon materials, deuteration reduces hyperfine-field strengths by only approximately 20%, which we attribute to the dominant contribution of the nitrogen nuclear spin to hyperfine interactions. At the same time, the decay rate of the DMDB triplet excited state is increased by almost a factor of two, in agreement with quantum-chemical calculations. The results demonstrate how the effects of deuteration can be extracted from ODMR spectra despite the strong influence of overlapping PP and TEP contributions.

DOI: 10.1103/sgwz-sr72

I. INTRODUCTION

Organic semiconductors give rise to a rich variety of spin-dependent processes that govern charge transport and light emission in organic light-emitting diodes (OLEDs). Because spin-orbit coupling is comparatively weak in most π-conjugated organic molecules, electronic spins retain coherence long enough for hyperfine interactions (HFIs) to drive singlet-triplet mixing in polaron pairs (PPs), whereby these interactions influence exciton formation rates [1–3]. Optically detected magnetic resonance (ODMR) provides a powerful means of probing such spin-dependent processes directly in operating devices, offering spectroscopic access to the underlying spin dynamics through changes in the electroluminescence (EL) intensity [4]. The linewidth of the ODMR response is directly sensitive to local hyperfine-field distributions. Although isotopic substitution is an obvious tool for testing for the influence of hyperfine fields on spin mixing in organic semiconductors, there are still only a few examples of this approach in the literature [5–9]. Most prior deuteration studies of OLEDs in general, and of ODMR line widths in particular, have focused on fluorescent π-conjugated polymers, where hyperfine fields are dominated by hydrogen nuclei. To directly test for hyperfine-field-induced mixing between singlet and triplet spin-pair states, it is desirable to employ dual fluorescence-phosphorescence-emitting OLED materials. Such compounds are dispersed in a host matrix and usually contain nitrogen atoms [10], which also contribute a significant HFI that cannot be mitigated. It therefore remains an open question how deuteration of the host, the guest, or both materials affects the ODMR line shape.

In a previous study on non-deuterated materials, we reported on fluorescence- and phosphorescence-resolved ODMR of OLEDs based on the dual-emitting molecule 11,12-dimethyldibenzo[*a,c*]phenazine (DMDB) [11], which exhibits well-separated fluorescent and phosphorescent spectral components when dispersed in a 4,4′-bis(*N*-carbazolyl)-1,1′-biphenyl (CBP) matrix [12] [the structures of the two compounds are shown in Figs. 1(c) and 1(d)]. We found that the ODMR response comprises two distinct processes: the PP mechanism, illustrated in Fig. 1(a), involving HFI-induced singlet-triplet mixing that yields a magnetic-field-dependent generation of excitons; and the TEP interaction, illustrated in Fig. 1(b), for which the HFI gives rise to a magnetic-field-dependent quenching of triplet excitons. Both the spin mixing in the PP mechanism [3] and the TEP process [13] are suppressed by a large external magnetic field. By modeling the exciton dynamics through the phase response of the lock-in-detected signal and by describing the magnetic-field dependence in the framework of a density-matrix stochas-

 ©2026 American Physical Society

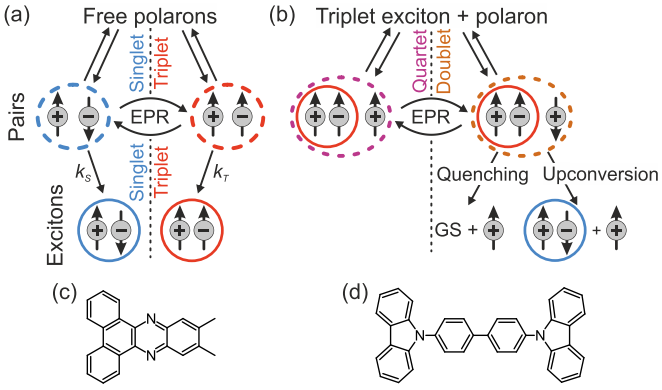


FIG. 1. Illustration of spin-dependent exciton generation via the polaron-pair (PP) mechanism and spin-dependent exciton recombination via the triplet-exciton polaron (TEP) mechanism. (a) Weakly coulombically coupled PPs (indicated by dashed ovals) can exist in either singlet (blue) or triplet (red) spin configurations. Hyperfine interactions (HFI) and the externally applied oscillating magnetic field that induce electron paramagnetic resonance (EPR) drive transitions between these spin states. Because singlet and triplet PPs recombine with different rates, k_S and k_T, this spin mixing results in a magnetic-field-dependent modulation of singlet and triplet exciton generation. (b) A triplet exciton can coulombically interact with an additional polaron to form a TEP precursor state (dashed ovals), which may adopt either a quartet (violet) or doublet (orange) spin configuration. As in the PP mechanism, the HFI and EPR drive transitions between these spin states. Because of the spin selection rules, recombination is only allowed from the doublet state, leading either to quenching into the ground state (GS) with the formation of a higher-energy polaron, or to an up-conversion process that produces an excited singlet state and a lower-energy polaron. In contrast, the quartet state dissociates back into a free triplet exciton and polaron. [(c) and (d)] Chemical structures of the dual-emitter guest molecule 11,12-dimethyldibenzo[a,c]phenazine (DMDB) and the host matrix 4,4′-bis(N-carbazolyl)-1,1′-biphenyl (CBP), which are both also present in perdeuterated form.

tic Liouville simulation, the experimentally observed ODMR signals could previously be rationalized quantitatively [11]. This analysis also revealed an up-conversion process, whereby triplet excitons are converted into singlet excitons through the TEP interaction.

The linewidth of the ODMR response is sensitive to the HFI arising from the coupling of electronic spins to nuclear magnetic moments [5–7]. However, because the PP and TEP mechanisms contribute to the ODMR signal with opposite signs [11], the resulting line shape is strongly convoluted. Therefore a rigorous deconvolution of the spectra is required before the hyperfine contributions can be reliably extracted from the deuteration series. The experimentally measured ODMR signals are modeled using the approach introduced in Ref. [11], which accounts for both the magnetic-field dependence and the relation between the in-phase and quadrature lock-in components associated with the exciton dynamics. The results reveal a deuteration-dependent modification of the hyperfine coupling, although the effect is much less pronounced than in the aforementioned studies on fluorescent OLED materials. This reduced sensitivity is likely due to the contribution of nitrogen nuclear spins, which are unaffected by deuteration. Deuteration also leads to a measurable reduction of the triplet lifetime of the guest, consistent with excited-state dynamics calculations that predict an enhancement of the reverse intersystem crossing rate. Deuteration has long been known to enhance OLED stability by lowering the vibrational frequency and hence retarding electrochemical decomposition processes [14], and has recently been explored extensively in the context of thermally activated delayed fluorescence OLEDs [15]. It has also been shown to improve circularly polarized emitters [16].

II. METHODS AND EXPERIMENTAL RESULTS

The devices used in this study are functionally equivalent to those described in Refs. [11,17]. In brief, the OLED stack consists of an ITO anode, hole- and electron-transport layers, a CBP:DMDB emitting layer, and a metal cathode. The emitting layer is made up of the dual-singlet-triplet emitter DMDB incorporated in a CBP matrix at a 3:97 weight ratio, deposited by thermal evaporation under vacuum. The active area of each device is 2.7 mm^2. Details of the device fabrication are given in Supplemental Material [18]. Both commercially available protonated materials and custom-synthesized deuterated analogs were employed. Details of the synthesis of the deuterated materials are given in the Supporting Information of Ref. [17]. As implemented in previous studies [11,12,17,19], fluorescence and phosphorescence were spectrally separated using a dichroic mirror with a cutoff at 552 nm, followed by a 600 nm long-pass filter in the phosphorescence channel. Additionally, a 445 nm long-pass filter placed before the dichroic mirror was used to suppress residual CBP emission. The emission was detected using a variable-gain photoreceiver (FEMTO, OE-200-SI).

A custom-built Helmholtz coil supplied a static magnetic field up to 30 mT, and three-axis Helmholtz coils were used to compensate for Earth's magnetic field. Devices were driven at a constant current density of 17.5 $mA\,cm^{-2}$. A radio-frequency (rf) magnetic field B_1 was generated by a coplanar waveguide (dimensions of the center conductor: 1.6 mm wide, 4 cm long, and 35 μm thick) located directly beneath the device and oriented perpendicular to the static field. At an rf source power of 10 W, we estimate $B_1 \approx 20$ μT. The rf signal was amplitude-modulated by a rectangular waveform with period T, which in this study was set to $T = 10.8$ ms. Fluorescence and phosphorescence signals were demodulated using separate lock-in amplifiers to obtain the in-phase and quadrature components of the rf-induced response. The rf carrier frequency was set to 280 MHz, resulting in ODMR resonances at static fields of approximately 10 mT. All measurements were performed at room temperature. The lock-in phase was referenced to the rise of the modulation waveform, and the time constant was 100 ms. The static field was swept from 0 to 20 mT.

The resulting ODMR spectra are displayed in Fig. 2. The leftmost column corresponds to the fully protonated sample and has previously been reported in Ref. [11]. The remaining columns correspond to perdeuteration of either host, guest, or both molecules. The in-phase component of the lock-in signal detected in the phosphorescence channel of the ODMR exhibits substantial differences in line shape between

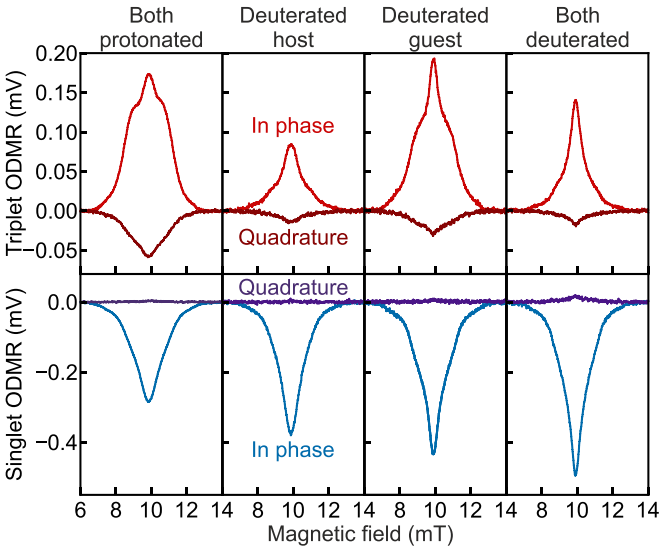


FIG. 2. Experimental ODMR spectra in the phosphorescence (upper panels, red) and fluorescence (lower panels, blue) channels, showing in-phase (lighter) and quadrature (darker) components. From left to right, the columns correspond to OLED samples with protonated host and guest, deuterated host only, deuterated guest only, and both host and guest deuterated. The leftmost data set is identical to the results reported in Ref. [11].

the different combinations of materials. The characteristic shoulder-like feature, most prominent in the fully protonated device, is strongly modified upon deuteration of either the host or the guest. In addition, the ratio of quadrature to in-phase signal amplitudes is largest for the fully protonated system. However, in contrast to reports of magnetic resonance experiments in other organic semiconductors [5–7], no clear narrowing of the resonance line upon deuteration is observed here.

The fluorescence channel also exhibits changes in line shape upon deuteration, although less pronounced than in the phosphorescence channel. Moreover, both in-phase and quadrature components show variations in overall signal intensity across the deuteration series. To account for these observations, both the magnetic-field effect and the role of lock-in detection must be characterized, as will be addressed in the following two sections.

III. LOCK-IN RESPONSE

The phosphorescence dynamics in this material system arise from a competition between direct electron-hole recombination on the guest and triplet-state energy transfer from the host to the guest. Because triplet states on the host CBP have lifetimes on the order of one second [20], energy transfer dominates the depopulation of CBP triplets. This behavior is also observed in transient electrophosphorescence measurements from Ref. [12], where an apparent phosphorescence lifetime of ∼97 ms can primarily be attributed to energy transfer. As demonstrated in our previous work [11] and reaffirmed here, the modulation frequency and lock-in detection scheme suppress the magnetic-field dependence of the triplet population of the host due to the combination of long triplet lifetime and

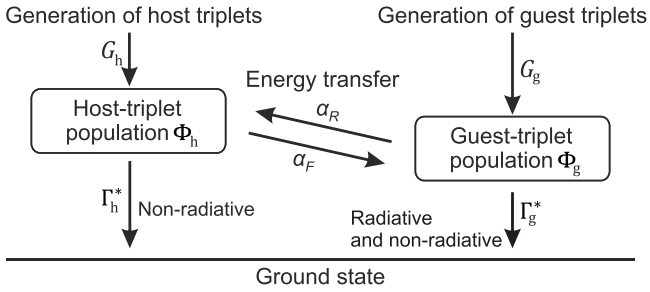


FIG. 3. Schematic visualization of the rate equations [Eq. (1)] adapted from Ref. [11]. The host and guest triplet populations are generated at rates G_h and G_g, and decay via the recombination rates Γ_h^* and Γ_g^*, respectively. Forward and reverse triplet energy transfer between host and guest are described by the rates α_F and α_R. The total depopulation rates entering into Eq. (1) are given by $\Gamma_g = \Gamma_g^* + \alpha_R$ and $\Gamma_h = \Gamma_h^* + \alpha_F$.

short modulation time. Accordingly, the measured magnetic-field effect primarily reflects direct triplet formation on the guest. The ratio of in-phase to quadrature lock-in components provides a model-based determination of the triplet lifetime of the guest, which is considerably shorter than the lifetime obtained from transient electrophosphorescence in Ref. [12].

The dynamics of the triplet population are described by the coupled rate equations (schematically visualized in Fig. 3)

$$\begin{aligned}\frac{d\Phi_h}{dt} &= G_h + \alpha_R\Phi_g - \Gamma_h\Phi_h,\\ \frac{d\Phi_g}{dt} &= G_g + \alpha_F\Phi_h - \Gamma_g\Phi_g,\end{aligned} \tag{1}$$

where G_h and G_g denote the generation rates, and Γ_h and Γ_g are the depopulation rates of host and guest triplets, respectively. Energy transfer is incorporated via the rate constants α_R and α_F representing guest-to-host (reverse) and host-to-guest (forward) transfer, where the depopulation due to energy transfer is included in the depopulation rates.

Magnetic fields modify the triplet population through magnetic-field-dependent variations of G_h, G_g, and Γ_g, which may be written as

$$\begin{aligned}G_g(t) &= G_g(B_0) + \delta G_g(B_0, B_1)F(t),\\ \Gamma_g(t) &= \Gamma_g(B_0) + \delta\Gamma_g(B_0, B_1)F(t),\\ G_h(t) &= G_h(B_0) + \delta G_h(B_0, B_1)F(t),\end{aligned} \tag{2}$$

where $F(t)$ is the rectangular modulation function defined as

$$\begin{aligned}F(t) &= 1,\ 0 \leqslant t < \frac{T}{2},\\ F(t) &= 0,\ \frac{T}{2} \leqslant t < T,\end{aligned} \tag{3}$$

and δG_g, δG_h, and $\delta\Gamma_g$ are small rf-induced perturbations.

Phase-sensitive lock-in detection yields the complex quantity

$$\mathcal{I} = \frac{2\pi}{\tau}\int_0^\tau dt\ \Phi_g(t)e^{ift}, \tag{4}$$

with $\tau \gg T$ the integration time and $f = 2\pi/T$ the modulation angular frequency. Evaluation of Eq. (4), as performed

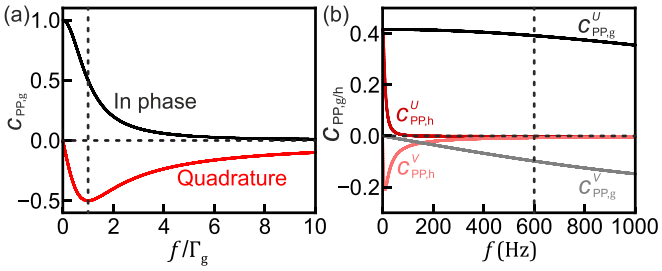


FIG. 4. (a) Calculated in-phase and quadrature components of the modulation-frequency-dependent scaling factor $c_{PP,g}$ from Eq. (6), using the parameters $\Gamma_g = 2400$ Hz, $\Gamma_h = 10$ Hz, $\alpha_F = 10$ Hz, and $\alpha_R = 0.001$ Hz (as determined in Ref. [11]). The frequency axis is normalized to the recombination rate Γ_g, and the dashed vertical line marks $f = \Gamma_g$. (b) Scaling factors associated with the PP process on the host, $c_{PP,h}$ (red), and on the guest, $c_{PP,g}$ (black), calculated with the same parameters. The dashed vertical line indicates the modulation frequency used in the experiment.

in Ref. [11], gives in-phase and quadrature components $U = \mathrm{Im}(\mathcal{I})$ and $V = \mathrm{Re}(\mathcal{I})$. These components depend sensitively on experimental conditions and may differ significantly in other regimes [21–23]. The resulting expressions are

$$U = \frac{\alpha_F(\Gamma_g\Gamma_h - f^2)}{(f^2+\Gamma_g^2)(f^2+\Gamma_h^2)}\delta G_h + \frac{\Gamma_g}{f^2+\Gamma_g^2}(\delta G_g - \Phi_{g,0}\delta\Gamma_g),$$
$$V = -\frac{\alpha_F f(\Gamma_g+\Gamma_h)}{(f^2+\Gamma_g^2)(f^2+\Gamma_h^2)}\delta G_h - \frac{f}{f^2+\Gamma_g^2}(\delta G_g - \Phi_{g,0}\delta\Gamma_g), \tag{5}$$

where $\Phi_{g,0} = (G_g\Gamma_h + \alpha_F G_h)/(\Gamma_g\Gamma_h - \alpha_F\alpha_R)$ is the steady-state triplet population on the guest. Notably, the frequency dependence associated with the guest PP mechanism (δG_g) and the TEP mechanism ($\delta\Gamma_g$) is identical, whereas the host PP mechanism (δG_h) exhibits a distinct dependence.

For clarity, scaling factors are introduced

$$c^U_{PP,h} = \frac{\alpha_F(\Gamma_g\Gamma_h - f^2)}{(f^2+\Gamma_g^2)(f^2+\Gamma_h^2)},\ c^V_{PP,h} = -\frac{\alpha_F f(\Gamma_g+\Gamma_h)}{(f^2+\Gamma_g^2)(f^2+\Gamma_h^2)},$$
$$c^U_{PP,g} = \frac{\Gamma_g}{f^2+\Gamma_g^2},\ c^V_{PP,g} = -\frac{f}{f^2+\Gamma_g^2},$$
$$c^U_{TEP} = c^U_{PP,g}\cdot\Phi_{g,0},\ c^V_{TEP} = c^V_{PP,g}\cdot\Phi_{g,0}, \tag{6}$$

allowing Eq. (5) to be rewritten compactly as

$$U = c^U_{PP,h}\cdot\delta G_h + c^U_{PP,g}\cdot\delta G_g + c^U_{TEP}\cdot\delta\Gamma_g,$$
$$V = c^V_{PP,h}\cdot\delta G_h + c^V_{PP,g}\cdot\delta G_g + c^V_{TEP}\cdot\delta\Gamma_g. \tag{7}$$

To illustrate the behavior of in-phase and quadrature components, the scaling factors were evaluated for various ratios of recombination rates to modulation frequency and are shown in Fig. 4(a). In the regime relevant to this work, the modulation-frequency dependence is relatively simple: the in-phase component gradually decreases with increasing frequency, whereas the magnitude of the quadrature component exhibits a maximum at $f = \Gamma_g$, decreasing thereafter, but less steeply than the in-phase response. In other regimes, the behavior can be considerably more complex, depending on the detailed system dynamics [23].

To compare $c_{PP,g}$ and $c_{PP,h}$, the modulation-frequency dependence of the scaling factors was calculated using the parameters from Ref. [11]. The results are shown in Fig. 4(b), where the dashed vertical line marks the modulation frequency employed in the measurements. Owing to the long host-triplet lifetime, the corresponding scaling factors are already reduced to small values at this frequency, indicating that the associated magnetic-field effect is strongly suppressed. While the triplets generated in the host may dominate the overall phosphorescence of the system, the modulation frequency used suppresses the detection of the associated magnetic-field effect, such that the ODMR signal is dominated by the PP and TEP processes directly on the emitter molecule.

IV. THEORETICAL MODELING OF THE EXPERIMENTAL DATA

As described in the previous section, the magnetic-field dependence of the triplet exciton population arises from two distinct contributions: a modification of the exciton generation rate via the PP mechanism [1,3,24–28] and a change of the triplet recombination rate via the TEP mechanism [3,4,13,29–32]. In the PP mechanism, weakly coulombically coupled electron-hole pairs form on the host or guest molecules in singlet- or triplet-like configurations. As illustrated in Fig. 1, these spin configurations can either dissociate back into separate polarons or recombine into excitons while conserving spin. Local hyperfine fields cause the spins within the PP to experience different effective magnetic fields, resulting in a time-dependent singlet-triplet mixing [2,3,5]. Application of an external magnetic field modifies this mixing and therefore changes the spin-dependent recombination probability of the PP ensemble. As a result, the exciton population becomes magnetic-field dependent.

The generation rate of triplet excitons is determined by the triplet fraction within the host (h) and guest (g) PP ensembles, corresponding to exciton formation on host molecules in the first case and on the emitter in the second. Following the approach introduced in Ref. [11], the two PP ensembles are represented by separate spin density matrices, ρ_h and ρ_g. The magnetic-field-dependent generation rates are then given by

$$G_h = r_{T,h}\mathrm{tr}(\rho_h\Pi_{T,h}),\ G_g = r_{T,g}\mathrm{tr}(\rho_g\Pi_{T,g}), \tag{8}$$

where $\Pi_{T,\mu}$ ($\mu = h, g$) denotes the projection operator onto the triplet manifold. The coefficients $r_{T,\mu}$ encompass all field-independent, material-specific contributions to exciton generation.

In the TEP mechanism, the spin-selective interaction between the guest triplet exciton and an additional polaron leads to a magnetic-field-dependent recombination rate of triplet excitons on the guest. The resulting TEP complex can adopt either a doublet or quartet configuration. Spin-conserving recombination into a molecular singlet, either in the ground state (quenching) [13,32] or in an excited state (up-conversion) [11,31], is allowed exclusively from the doublet manifold, whereas states in the quartet manifold dissociate without recombination [13,30,32].

The TEP ensemble is represented by a spin density matrix ϱ, such that the population decay of triplet excitons is

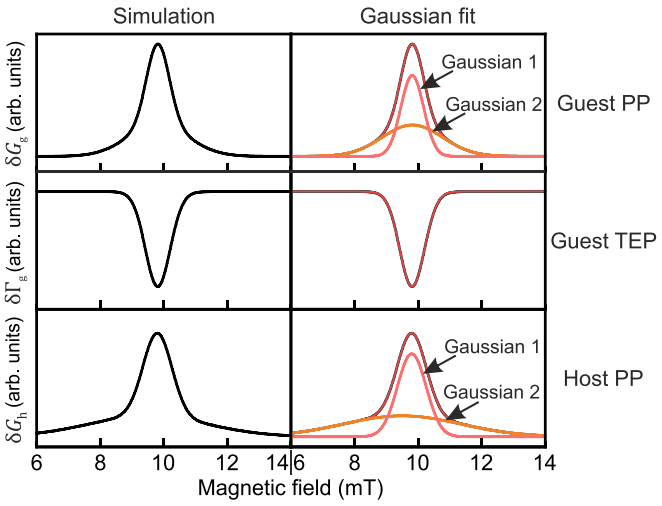


FIG. 5. Simulated line shapes of the PP mechanism on the guest ($B_{\mathrm{hf},e} = 0.94$ mT, $B_{\mathrm{hf,h}} = 0.35$ mT), the PP mechanism on the host ($B_{\mathrm{hf},e} = 1.82$ mT, $B_{\mathrm{hf,h}} = 0.94$ mT), and the TEP mechanism ($B_{\mathrm{hf,h}} = 0.355$ mT) (left) using the parameters from Ref. [11] that describe the fully protonated CBP:DMDB OLED. The right column shows the corresponding Gaussian fits of the data generated by the simulations. A double-Gaussian profile is used for the PP mechanism and a single-Gaussian profile for the TEP mechanism.

expressed as

$$\Gamma_{\mathrm{g}}\Phi_{\mathrm{g}} = r_{\mathrm{D}}\mathrm{tr}(\varrho\Pi_{\mathrm{D}}) + \Gamma_{\mathrm{g}}^{'}\Phi_{\mathrm{g}}, \tag{9}$$

where Π_{D} denotes the projection operator onto the doublet manifold and r_{D} parameterizes the field-dependent doublet recombination channel. The term $\Gamma_{\mathrm{g}}^{'}$ accounts for the field-independent contribution to the triplet decay rate, allowing the TEP-induced magnetic-field dependence to be isolated.

Using the stochastic Liouville equations,

$$\begin{aligned}\frac{d\rho_\mu}{dt} &= \Lambda_\mu 1_{4\times4} + i[\rho_\mu,\ H_{\mathrm{PP},\mu}] + \mathcal{R}_{\mathrm{dr}}\{\rho_\mu\} + \mathcal{R}_{\mathrm{sl}}\{\rho_\mu\},\\ \frac{d\varrho}{dt} &= \Lambda_{\mathrm{TEP}} 1_{6\times6} + i[\varrho,\ H_{\mathrm{TEP}}] + \mathcal{R}_{\mathrm{dr}}\{\varrho\} + \mathcal{R}_{\mathrm{sl}}\{\varrho\},\end{aligned} \tag{10}$$

the time evolution of the density matrices ρ_μ ($\mu = \mathrm{h}, \mathrm{g}$) and ϱ for the PP and TEP ensembles, respectively, can be described. The first terms represent the generation of PP and TEP complexes with rates Λ_μ and Λ_{TEP}. The second terms reflect the coherent spin dynamics governed by the respective Hamiltonians $H_{\mathrm{PP},\mu}$ and H_{TEP}. Dissociation and recombination processes are captured by the operator $\mathcal{R}_{\mathrm{dr}}$, while spin-lattice relaxation is described by $\mathcal{R}_{\mathrm{sl}}$.

A detailed analysis of Eqs. (8)–(10) is provided in Ref. [11], where the corresponding solutions are used to numerically compute the ODMR signals arising from the field dependence of δG_{g}, δG_{h}, and $\delta\Gamma_{\mathrm{g}}$. Figure 5 shows the calculated individual contributions using the parameter set employed to fit the fully protonated CBP:DMDB OLEDs reported in Ref. [11]. For visualization purposes, a Gaussian fit to the simulated data is included, highlighting the resulting line-shape characteristics.

The simulations reveal a double-Gaussian line shape for the PP mechanism, reflecting the hyperfine field distributions associated with electron and hole polarons, consistent with previous reports in the literature [6,33–35]. In contrast, the TEP contribution exhibits a single-Gaussian profile, as the model assumes that TEP predominantly involves either the electron or hole polaron. Deviations from simple Gaussian behavior are expected when dipolar or exchange interactions between the PP constituents become significant, which is not the case for the system studied here [11]. The corresponding dipolar D_d and exchange couplings J inferred for CBP:DMDB in Ref. [11], $D_d = 0.22$ mT and $J = 0.02$ mT, lie well below the hyperfine-field distribution widths reported in Table I, justifying the use of the weakly coupled limit in the present analysis.

The relative displacement of the two Gaussians associated with the PP mechanism leads to an asymmetric overall line shape. This shift can arise from slightly different electron and hole polaron g-factors, as well as from hyperfine components perpendicular to the externally applied magnetic field, which modify the resonance condition, depending on the magnitude of the local hyperfine fields [11]. A direct resonance contribution from the triplet excitons within the TEP mechanism is not expected in this field regime, because the zero-field splitting parameters significantly exceed the resonance field [11,36].

In addition to identifying the appropriate parameters for calculating the resonances from the density-matrix simulations, the correct scaling factors [Eq. (6)] must be determined. Because the density-matrix calculations inherently carry an uncertainty in the absolute amplitudes of the magnetic-field effects, the absolute signal strengths cannot be assigned unambiguously. Instead, the ratio of in-phase to quadrature scaling factors is considered,

$$\frac{c^U_{\mathrm{PP,h}}}{c^V_{\mathrm{PP,h}}} = -\frac{\Gamma_{\mathrm{g}}\Gamma_{\mathrm{h}} - f^2}{f(\Gamma_{\mathrm{g}} + \Gamma_{\mathrm{h}})},\ \frac{c^U_{\mathrm{PP,g}}}{c^V_{\mathrm{PP,g}}} = \frac{c^U_{\mathrm{TEP}}}{c^V_{\mathrm{TEP}}} = -\frac{\Gamma_{\mathrm{g}}}{f}, \tag{11}$$

TABLE I. Parameter sets used for fitting the experimental data shown in Fig. 6. $B_{\mathrm{hf},e}$ and $B_{\mathrm{hf,h}}$ denote the widths of the Gaussian hyperfine-field distributions of electron and hole polarons. Also listed is the recombination rate of guest triplets Γ_{g}, as determined from the ratio of the in-phase and quadrature triplet ODMR signals.

		Both protonated	Deuterated host	Deuterated guest	Both deuterated
δG_{g}	$B_{\mathrm{hf},e}$(mT)	0.94	0.94	0.94	0.85
	$B_{\mathrm{hf,h}}$(mT)	0.35	0.34	0.30	0.27
$\delta\Gamma_{\mathrm{g}}$	$B_{\mathrm{hf,h}}$(mT)	0.355	0.343	0.305	0.271
	Γ_{g} (kHz)	2.4	3.8	3.9	4.7

from which it becomes evident that these ratios depend solely on the recombination rates of the host and guest triplets and on the modulation frequency. Moreover, Eq. (11) shows that the ratio of in-phase to quadrature signals is *identical* for both the TEP and the PP mechanisms acting on the guest. Because the modulation frequency f is fixed experimentally, the ratio of in-phase to quadrature components provides a direct measure of the corresponding recombination rates. This conclusion means that the guest-triplet recombination rate Γ_g can be inferred from the ratio of measured in-phase and quadrature signals, without reliance on the absolute amplitudes from the density-matrix calculations.

Because a large number of parameters influence the line shape, fitting the calculated response to experimental data may appear to be underdetermined. However, the constraint imposed by the known relation between in-phase and quadrature components significantly reduces the accessible parameter space. Specifically, the fit is subject to three explicit constraints: (i) the magnetic-field parameters governing δG_h, δG_g, and $\delta\Gamma_g$ must be identical for the in-phase and quadrature triplet ODMR signals of a given sample, with only the scaling factors allowed to vary; (ii) the in-phase to quadrature ratio of the scaling factors must be the same for the TEP and the PP mechanism acting on the guest, as enforced by Eq. (11); and (iii) the singlet ODMR of the same sample must be described by the same magnetic-field-dependent parameters as the triplet ODMR, with only the scaling factors differing. These combined constraints lead to a fitting procedure that yields a well-constrained and self-consistent parameter set, enabling a reliable extraction of the underlying hyperfine-field distributions.

The resulting fits of the simulated data to the experimental spectra are shown in Fig. 6. For each combination of materials, the in-phase triplet ODMR, quadrature triplet ODMR, and singlet ODMR spectra can be reproduced simultaneously using a single density-matrix parameter set. This agreement demonstrates that all spectra of a given sample are consistently described by identical hyperfine-field strengths. The parameters used in the simulations are summarized in Table I.

The quadrature singlet ODMR was not included in the fitting procedure as its signal-to-noise ratio was insufficient to reliably extract parameters since the singlet lifetime is so much shorter than that of the triplet. Although the PP contribution on the host is required to correctly describe the difference between in-phase and quadrature line shapes, its overall contribution is weak, preventing an unambiguous determination of the associated hyperfine-field parameters. Consequently, while the host PP process was included in the simulations, the extracted parameters cannot be uniquely assigned. This ambiguity is consistent with Fig. 4, which shows that the host PP contribution is negligible in the in-phase component and remains very small in the quadrature component due to its already strongly reduced amplitude.

A comparison of the extracted hyperfine-field parameters for the different combinations of materials shows that deuteration indeed reduces the hyperfine fields, although the effect is relatively weak. Deuterating the host alone results in only a minor decrease in the hyperfine fields associated with the hole polaron in both the PP and TEP processes. In contrast,

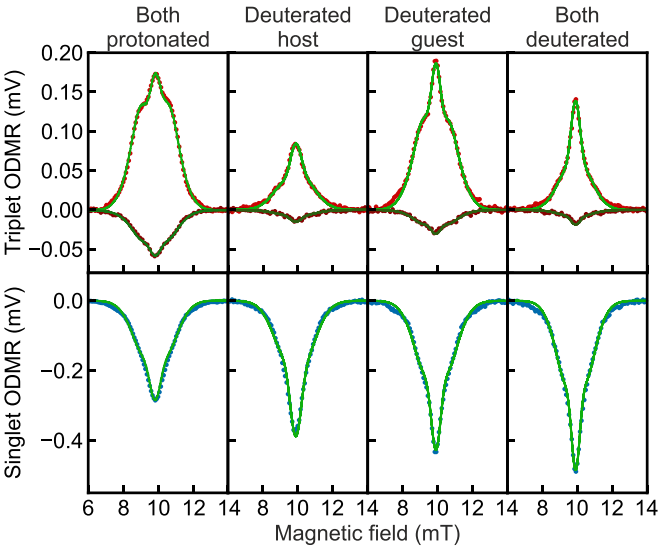


FIG. 6. Experimental ODMR signals in phosphorescence (top, red dots) and fluorescence (bottom, blue dots). For the phosphorescence channel, both the in-phase and quadrature components are shown (darker dots indicate the quadrature signal). From left to right, the columns correspond to OLED samples with protonated host and guest, deuterated host only, deuterated guest only, and both host and guest deuterated. The green lines display simulated line shapes that provide the best match to the experimental data. The simulation shown in the leftmost column corresponds to the result previously reported in Ref. [11].

deuterating the guest produces a more pronounced reduction in the hole-polaron hyperfine-field distribution. When both host and guest are deuterated, the strongest reduction is observed, now affecting both the electron and hole polarons. Between the fully protonated and fully deuterated devices, the hyperfine-field strengths decrease by approximately 24% for the hole polaron and by approximately 10% for the electron polaron.

Table I also lists the recombination rate of the guest triplets, Γ_g, obtained from the ratio of the in-phase to quadrature triplet ODMR signals [see Eq. (11)]. A clear increase in Γ_g with deuteration is observed: in the fully deuterated device, Γ_g is approximately twice the value found for the fully protonated device. The trend is monotonic across the different combinations of materials, with deuteration of either host or guest yielding intermediate values. The observed dependence of Γ_g on host deuteration indicates that the guest-triplet decay dynamics are influenced not only by intrinsic DMDB properties but also by host-mediated transfer and annihilation pathways.

V. DISCUSSION

A central finding of this work is that the substantial differences in line shape observed for the differently deuterated samples appear counterintuitive, especially given that the parameter sets required to reproduce these changes vary only weakly. Likewise, the singlet ODMR exhibits a markedly different resonance from the triplet ODMR despite being described by identical hyperfine-field parameters. The origin of

these pronounced spectral changes is therefore not primarily rooted in modifications of the intrinsic parameters of the individual mechanisms, such as hyperfine-field strengths or dipolar and exchange coupling strengths of the polarons involved, but rather in the relative amplitudes of the TEP and PP mechanisms. Because these mechanisms enter the total signal with opposite signs, even small variations in their amplitude ratio lead to substantial alterations in the resulting line shape.

The singlet ODMR is also influenced by the TEP mechanism via up-conversion, as evidenced in Ref. [11] by a TEP-shaped component in the fluorescence ODMR opposite in sign to the TEP contribution in the phosphorescence ODMR. However, since up-conversion is endothermic, the number of up-converted triplets is significantly smaller than the number of triplets quenched. Therefore the impact of the TEP mechanism on the singlet ODMR is much weaker, and the resulting lines more closely approximate the simple double-Gaussian profile of the PP mechanism. Nonetheless, deviations from a purely double-Gaussian behavior remain discernible upon closer inspection.

Deuteration of the materials influences the hyperfine-field parameters, as expected from the smaller nuclear magnetic moment of deuterium compared to hydrogen (by approximately a factor of three [37]). However, the resulting reduction in hyperfine fields remains modest, amounting to only 10%–24% between the fully protonated and fully deuterated devices (see Table I). In contrast to reports on fluorescent polymers [5–7], where deuteration leads to clearly resolved narrowing of the ODMR line widths, no comparable narrowing is discernible here. A key difference in the present material system is the presence of nitrogen atoms in both host and guest molecules. Nitrogen carries a nuclear magnetic moment, which remains unaffected by deuteration. Moreover, the nonbonding (n) orbitals contributed by the nitrogen atoms in the DMDB guest give rise to $n\pi^*$ excited states that are associated with spin-orbit coupling and are hence crucial for enabling phosphorescence [38]. Substantial localization of the polaron wave function on these nitrogen sites is therefore to be expected, causing the observed hyperfine fields to be dominated by the nitrogen nuclear magnetic moment. This observation is consistent with our earlier study of magnetoresistance and magnetoelectroluminescence in the small-field regime in the same material system, where the respective line shapes were likewise only weakly affected by deuteration [17].

A puzzling aspect arises when considering the effect of selectively deuterating either the host or the guest molecules on the extracted hyperfine-field parameters. In Ref. [11], it was proposed that the hyperfine-field distribution associated with the TEP mechanism reflects that of the hole polaron, since the host material CBP is known to be an effective hole conductor [39]. Experimentally, however, we find that deuteration of the host has a vanishingly small influence on the resonance spectra, whereas deuteration of the emitter leads to a measurable reduction of the hyperfine field of the hole polaron, with the strongest reduction observed upon deuterating both host and guest.

Based on the above discussion, one would instead expect the opposite behavior: because the hyperfine fields on the guest are dominated by the nitrogen nuclear magnetic moment and are therefore largely immune to deuteration, deuterating the host should have produced a stronger effect. The present result therefore suggests that, in the PP spin-mixing process, the hole polaron resides predominantly on the emitter molecule, as evidenced by its sensitivity to emitter deuteration. Given the low guest concentration, this observation would imply that the electron polaron resides on the host molecule. However, this conclusion conflicts with the almost negligible change in the electron hyperfine field upon deuterating the host. Moreover, the TEP mechanism is linked to the guest triplet lifetime, implying that the triplet exciton in the TEP complex is localized on the guest and therefore that the hole polaron in the TEP state must reside in the host. A consistent resolution of these observations is that the nitrogen nuclei of CBP also contribute substantially to the hyperfine fields experienced by polarons residing on the host, with electron and hole polarons sampling these nitrogen sites differently. In this picture, both PP and TEP HFI distributions are buffered by contributions from nitrogen on whichever molecule the polaron resides on, so that C-H $\rightarrow$ C-D substitution probes only the residual contribution of the protons to the HFI. This hypothesis can be tested directly by repeating the experiment on a nitrogen-free host-guest combination, where deuteration is expected to reproduce the much larger reduction in line width reported for fluorescent polymers [5–7]. Furthermore, the observation that deuteration of both the host and the guest gives rise to the strongest reduction of the hyperfine fields is consistent with a scenario in which the hole polaron resides, at least partially, at the host-guest interface, both in the PP mechanism on the guest and in the TEP mechanism.

The observed increase in the recombination rate upon deuteration can also be rationalized by excited-state dynamics calculations performed within the ORCA quantum-chemistry package, which used electronic states and vibrational modes derived from (time-dependent) density functional theory to estimate the reverse intersystem crossing (rISC) rates of the guest molecule DMDB (see Supplemental Material [18]). These calculations predict an enhancement of the rISC rate by roughly a factor of 5 upon deuteration. Since the rISC process contributes to the overall triplet recombination pathway, the guest triplet recombination rate Γ_g is affected likewise. The experimentally observed increase in Γ_g is therefore consistent with the predictions from theory, although a quantitative comparison is not possible because the present experiment is not selectively sensitive to the rISC rate alone and also incorporates other triplet decay channels such as annihilation processes like TEP and triplet-triplet annihilation. Because deuteration is known to alter OLED stability by retarding electrochemical decomposition [14], it may also affect the efficiency of these annihilation processes. The combined effect of a deuteration-dependent rISC rate and altered annihilation dynamics offers a possible explanation for why the experimentally observed enhancement of Γ_g is smaller than the bare rISC enhancement predicted in our calculations.

As discussed by Siebrand [40] and by Lin and Bersohn [41], vibronic relaxation is influenced by deuteration since C-H and C-D stretching modes play a key role in nonradiative decay, so that deuteration increases the triplet lifetime. In the present system, however, triplet decay is also influenced by radiative phosphorescence, such that these mechanisms

are expected to superimpose. Consequently, the increase in relaxation rate upon deuteration observed here is not in direct contradiction to the earlier study [41].

VI. CONCLUSIONS AND OUTLOOK

In summary, we performed ODMR experiments on the dual singlet-triplet emitting material system CBP:DMDB and observed ODMR signals in both the fluorescence and phosphorescence channels for devices with either a deuterated host, a deuterated guest, or both materials deuterated. The strongly convoluted resonances could be disentangled by combining lock-in detection of the ODMR with a theoretical framework that accounts for both the phase response of the lock-in-detected signals and the magnetic-field-dependent line shapes of the PP and TEP mechanisms.

Fitting the experimental data with the simulated spectra enabled the extraction of the hyperfine-field parameters as well as the recombination rate of guest triplet excitons, which is fundamentally different from the overall electroluminescence lifetime obtained from transient electrophosphorescence measurements of 97 ms [12]. We observe that deuteration affects both the hyperfine fields and the guest triplet recombination rate. The influence of deuteration on the hyperfine fields is limited to a reduction of approximately 10%–24% between the fully protonated and fully deuterated devices, which is significantly less than the reductions reported for fluorescent polymer-based systems [5–7]; from the ratio of the nuclear magnetic moments and hyperfine-coupling strengths of hydrogen and deuterium, one would expect an approximately threefold reduction [37]. This deviation can be rationalized by the dominant contribution of nitrogen nuclear spins to the HFI in both the host and guest molecules.

In contrast, the guest-triplet recombination rate increases noticeably upon deuteration. This trend is consistent with excited-state dynamics calculations, which predict enhanced rISC upon deuteration. While the absolute rates cannot be compared directly, the qualitative agreement supports this interpretation. Selective deuteration of host or guest yields hyperfine-field reductions that, taken at face value, place the hole polaron on different molecules in the PP and TEP mechanisms. We propose that this apparent contradiction is resolved by a substantial contribution of the nitrogen nucleus to the host hyperfine field, with electron and hole polarons sampling the host nitrogen differently. This hypothesis can be tested directly in a nitrogen-free analog of the present material system, where deuteration is expected to produce the much larger line width reduction reported for fluorescent polymers [5–7]. However, removing nitrogen from the guest emitter will obviously inhibit the dual singlet-triplet emission without resorting to a suitable substitution to activate $n\pi^*$ transitions.

To further refine the analysis of these spin-dependent processes, future experiments could map the modulation-frequency-dependent scaling factors over a broad frequency range, thereby directly testing the proposed exciton dynamics of the system. In addition, employing nitrogen-free dual-emitting molecules together with nitrogen-free host materials would enable more definitive conclusions regarding the localization of electron and hole polarons in the PP and TEP mechanisms, as the influence of deuteration on the hyperfine-field parameters is expected to be significantly stronger in the absence of nitrogen nuclear spins. Furthermore, time-resolved ODMR experiments, analogous to those previously demonstrated in electrically detected magnetic resonance (EDMR) [42], would allow the spectral line shapes to be analyzed as a function of time following an rf excitation pulse, providing a more direct and quantitative assessment of the underlying spin and recombination dynamics.

ACKNOWLEDGMENTS

This work is funded by the Deutsche Forschungsgemeinschaft (DFG, German Research Foundation) (project ID 314695032-SFB 1277, subproject B03). Also funded by the DFG as part of the German Excellence Strategy–EXC3112/1–533767171 (Center for Chiral Electronics). C.B. acknowledges funding from the Federal Ministry of Education and Research (BMBF) and the Ministry of Culture and Science of the German State of North Rhine-Westphalia (MKW) under the Excellence Strategy of the Federal Government and the Länder (RWTH JPI Fellowship), as well as funding from the MKW via the NRW Rückkehrprogramm.

DATA AVAILABILITY

All raw data from the measurements, the simulations, and the quantum-chemical calculations are available at [43].

[1] U. E. Steiner and T. Ulrich, Magnetic field effects in chemical kinetics and related phenomena, Chem. Rev. **89**, 51 (1989).

[2] V. N. Prigodin, J. D. Bergeson, D. M. Lincoln, and A. J. Epstein, Anomalous room temperature magnetoresistance in organic semiconductors, Synth. Met. **156**, 757 (2006).

[3] A. J. Schellekens, W. Wagemans, S. P. Kersten, P. A. Bobbert, and B. Koopmans, Microscopic modeling of magnetic-field effects on charge transport in organic semiconductors, Phys. Rev. B **84**, 075204 (2011).

[4] J. Shinar, Optically detected magnetic resonance studies of luminescence-quenching processes in π-conjugated materials and organic light-emitting devices, Laser Photonics Rev. **6**, 767 (2012).

[5] T. D. Nguyen, G. Hukic-Markosian, F. Wang, L. Wojcik, X.-G. Li, E. Ehrenfreund, and Z. V. Vardeny, Isotope effect in spin response of π-conjugated polymer films and devices, Nat. Mater. **9**, 345 (2010).

[6] D. M. Stoltzfus, G. Joshi, H. Popli, S. Jamali, M. Kavand, S. Milster, T. Grünbaum, S. Bange, A. Nahlawi, M. Y. Teferi, S. I. Atwood, A. E. Leung, T. A. Darwish, H. Malissa, P. L. Burn, J. M. Lupton, and C. Boehme, Perdeuteration of poly[2-methoxy-5-(2′-ethylhexyloxy)-1,4-phenylenevinylene] (d-MEH-PPV): Control of microscopic charge-carrier spin–spin coupling and of magnetic-field effects in optoelectronic devices, J. Mater. Chem. C **8**, 2764 (2020).

[7] S. Milster, T. Grünbaum, S. Bange, S. Kurrmann, H. Kraus, D. M. Stoltzfus, A. E. Leung, T. A. Darwish, P. L. Burn, C.

Boehme, and J. M. Lupton, Perdeuterated conjugated polymers for ultralow-frequency magnetic resonance of OLEDs, Angew. Chem. Int. Ed. **59**, 9388 (2020).

[8] T. D. Nguyen, T. P. Basel, Y. J. Pu, X. G. Li, E. Ehrenfreund, and Z. V. Vardeny, Isotope effect in the spin response of aluminum tris(8-hydroxyquinoline) based devices, Phys. Rev. B **85**, 245437 (2012).

[9] N. J. Rolfe, M. Heeney, P. B. Wyatt, A. J. Drew, T. Kreouzis, and W. P. Gillin, Elucidating the role of hyperfine interactions on organic magnetoresistance using deuterated aluminium tris(8-hydroxyquinoline), Phys. Rev. B **80**, 241201 (2009).

[10] D. Chaudhuri, E. Sigmund, A. Meyer, L. Röck, P. Klemm, S. Lautenschlager, A. Schmid, S. R. Yost, T. Van Voorhis, S. Bange, S. Höger, and J. M. Lupton, Metal-Free OLED triplet emitters by side-stepping Kasha's rule, Angew. Chem. Int. Ed. **52**, 13449 (2013).

[11] F. Braun, T. Scharff, T. Grünbaum, E. Schmid, S. Bange, V. V. Mkhitaryan, and J. M. Lupton, Polaron-induced upconversion from triplets to singlets: Fluorescence- and phosphorescence-resolved optically detected magnetic resonance of OLEDs, Phys. Rev. Appl. **20**, 044076 (2023).

[12] W. Ratzke, S. Bange, and J. M. Lupton, Direct Detection of singlet-triplet interconversion in OLED magnetoelectroluminescence with a metal-free fluorescence-phosphorescence dual emitter, Phys. Rev. Appl. **9**, 054038 (2018).

[13] V. Ern and R. E. Merrifield, Magnetic field effect on triplet exciton quenching in organic crystals, Phys. Rev. Lett. **21**, 609 (1968).

[14] C. C. Tong and K. C. Hwang, Enhancement of OLED efficiencies and high-voltage stabilities of light-emitting materials by deuteration, J. Phys. Chem. C **111**, 3490 (2007).

[15] S. Jung, W.-L. Cheung, S.-j. Li, M. Wang, W. Li, C. Wang, X. Song, G. Wei, Q. Song, S. S. Chen, W. Cai, M. Ng, W. K. Tang, and M.-C. Tang, Enhancing operational stability of OLEDs based on subatomic modified thermally activated delayed fluorescence compounds, Nat. Commun. **14**, 6481 (2023).

[16] Z. Chen, M. Huang, C. Zhong, M. Wang, J. Miao, and C. Yang, Deuteration promotes circularly polarized light emission by suppression of vibration, Nat. Commun. **17**, 678 (2026).

[17] F. Braun, T. Dollinger, S. Bange, V. V. Mkhitaryan, C. Knabbe, N. Schmickler, S. Höger, and J. M. Lupton, Effect of hyperfine interactions in highly anisotropic organic light-emitting diode magnetoelectroluminescence resolved in the singlet and triplet recombination channels, Phys. Rev. B **113**, 075202 (2026).

[18] See Supplemental Material at http://link.aps.org/supplemental/10.1103/sgwz-sr72 for details on the rISC calculations, additional parameter sets, and device fabrication, which also includes Refs. [44–70].

[19] T. Scharff, W. Ratzke, J. Zipfel, P. Klemm, S. Bange, and J. M. Lupton, Complete polarization of electronic spins in OLEDs, Nat. Commun. **12**, 2071 (2021).

[20] M. A. Baldo and S. R. Forrest, Transient analysis of organic electrophosphorescence: I. Transient analysis of triplet energy transfer, Phys. Rev. B **62**, 10958 (2000).

[21] E. Lifshitz, L. Fradkin, A. Glozman, and L. Langof, Optically detected magnetic resonance studies of colloidal semiconductor nanocrystals, Annu. Rev. Phys. Chem. **55**, 509 (2004).

[22] D. M. G. Leite, A. Batagin-Neto, O. Nunes-Neto, J. A. Gómez, and C. F. O. Graeff, Electrically detected magnetic resonance modeling and fitting: An equivalent circuit approach, J. Appl. Phys. **115**, 034510 (2014).

[23] S.-Y. Lee, S. Paik, D. R. McCamey, and C. Boehme, Modulation frequency dependence of continuous-wave optically/electrically detected magnetic resonance, Phys. Rev. B **86**, 115204 (2012).

[24] H. Kraus, S. Bange, F. Frunder, U. Scherf, C. Boehme, and J. M. Lupton, Visualizing the radical-pair mechanism of molecular magnetic field effects by magnetic resonance induced electrofluorescence to electrophosphorescence interconversion, Phys. Rev. B **95**, 241201(R) (2017).

[25] S. Jamali, V. V. Mkhitaryan, H. Malissa, A. Nahlawi, H. Popli, T. Grünbaum, S. Bange, S. Milster, D. M. Stoltzfus, A. E. Leung, T. A. Darwish, P. L. Burn, J. M. Lupton, and C. Boehme, Floquet spin states in OLEDs, Nat. Commun. **12**, 465 (2021).

[26] W. J. Baker, T. L. Keevers, J. M. Lupton, D. R. McCamey, and C. Boehme, Slow hopping and spin dephasing of coulombically bound polaron pairs in an organic semiconductor at room temperature, Phys. Rev. Lett. **108**, 267601 (2012).

[27] K. Kanemoto, S. Hatanaka, K. Kimura, Y. Ueda, and H. Matsuoka, Field-induced dissociation of electron-hole pairs in organic light emitting diodes monitored directly from bias-dependent magnetic resonance techniques, Phys. Rev. Mater. **1**, 022601 (2017).

[28] J. E. Lawrence, A. M. Lewis, D. E. Manolopoulos, and P. J. Hore, Magnetoelectroluminescence in organic light-emitting diodes, J. Chem. Phys. **144**, 214109 (2016).

[29] P. Desai, P. Shakya, T. Kreouzis, W. P. Gillin, N. A. Morley, and M. R. J. Gibbs, Magnetoresistance and efficiency measurements of Alq_3-based OLEDs, Phys. Rev. B **75**, 094423 (2007).

[30] T. L. Keevers, W. J. Baker, and D. R. McCamey, Theory of exciton-polaron complexes in pulsed electrically detected magnetic resonance, Phys. Rev. B **91**, 205206 (2015).

[31] A. Obolda, Q. M. Peng, C. Y. He, T. Zhang, J. J. Ren, H. W. Ma, Z. G. Shuai, and F. Li, Triplet–polaron-interaction-induced upconversion from triplet to singlet: A possible way to obtain highly efficient OLEDs, Adv. Mater. **28**, 4740 (2016).

[32] R. E. Merrifield, Magnetic effects on triplet exciton interactions, Pure Appl. Chem. **27**, 481 (1971).

[33] H. Malissa, R. Miller, D. L. Baird, S. Jamali, G. Joshi, M. Bursch, S. Grimme, J. van Tol, J. M. Lupton, and C. Boehme, Revealing weak spin-orbit coupling effects on charge carriers in a π -conjugated polymer, Phys. Rev. B **97**, 161201 (2018).

[34] G. Joshi, R. Miller, L. Ogden, M. Kavand, S. Jamali, K. Ambal, S. Venkatesh, D. Schurig, H. Malissa, J. M. Lupton, and C. Boehme, Separating hyperfine from spin-orbit interactions in organic semiconductors by multi-octave magnetic resonance using coplanar waveguide microresonators, Appl. Phys. Lett. **109**, 103303 (2016).

[35] H. Malissa, M. Kavand, D. P. Waters, K. J. van Schooten, P. L. Burn, Z. V. Vardeny, B. Saam, J. M. Lupton, and C. Boehme, Room-temperature coupling between electrical current and nuclear spins in OLEDs, Science **345**, 1487 (2014).

[36] N. M. Atherton, *Electron Spin Resonance* (Halsted, New York, 1973).

[37] G. H. Fuller, Nuclear spins and moments, J. Phys. Chem. Ref. Data **5**, 835 (1976).

[38] W. Ratzke, L. Schmitt, H. Matsuoka, C. Bannwarth, M. Retegan, S. Bange, P. Klemm, F. Neese, S. Grimme, O. Schiemann, J. M. Lupton, and S. Höger, Effect of conjugation pathway in metal-free room-temperature dual singlet–triplet emitters for organic light-emitting diodes, J. Phys. Chem. Lett. **7**, 4802 (2016).

[39] N. Liu, S. Mei, D. Sun, W. Shi, J. Feng, Y. Zhou, F. Mei, J. Xu, Y. Jiang, and X. Cao, Effects of charge transport materials on blue fluorescent organic light-emitting diodes with a host-dopant system, Micromachines **10**, 344 (2019).

[40] W. Siebrand and D. F. Williams, Isotope rule for radiationless transitions with an application to triplet decay in aromatic hydrocarbons, J. Chem. Phys. **46**, 403 (1967).

[41] S. H. Lin and R. Bersohn, Effect of partial deuteration and temperature on triplet-state lifetimes, J. Chem. Phys. **48**, 2732 (1968).

[42] W. J. Baker, D. R. McCamey, K. J. van Schooten, J. M. Lupton, and C. Boehme, Differentiation between polaron-pair and triplet-exciton polaron spin-dependent mechanisms in organic light-emitting diodes by coherent spin beating, Phys. Rev. B **84**, 165205 (2011).

[43] F. Braun, V. V. Mkhitaryan, S. Bange, M. Pauls, S. Höger, C. Bannwarth, and J. M. Lupton, Data archive of "Effect of deuteration in fluorescence- and phosphorescence-resolved optically detected magnetic resonance of metal-free dual singlet-triplet emitting OLEDs," [Dataset], 2026, https://doi.org/10.5283/epub.80534.

[44] S. Grimme, J. G. Brandenburg, C. Bannwarth, and A. Hansen, Consistent structures and interactions by density functional theory with small atomic orbital basis sets, J. Chem. Phys. **143**, 054107 (2015).

[45] B. de Souza, F. Neese, and R. Izsák, On the theoretical prediction of fluorescence rates from first principles using the path integral approach, J. Chem. Phys. **148**, 034104 (2018).

[46] B. de Souza, G. Farias, F. Neese, and R. Izsák, Predicting phosphorescence rates of light organic molecules using time-dependent density functional theory and the path integral approach to dynamics, J. Chem. Theory Comput. **15**, 1896 (2019).

[47] F. Neese, F. Wennmohs, U. Becker, and C. Riplinger, The ORCA quantum chemistry program package, J. Chem. Phys. **152**, 224108 (2020).

[48] F. Neese, Software Update: The ORCA Program System—Version 6.0, WIREs Computational Mol. Sci. **15**, e70019 (2025).

[49] Q. Peng, Y. Niu, Q. Shi, X. Gao, and Z. Shuai, Correlation function formalism for triplet excited state decay: Combined spin–orbit and nonadiabatic couplings, J. Chem. Theory Comput. **9**, 1132 (2013).

[50] M. Hagai, N. Inai, T. Yasuda, K. J. Fujimoto, and T. Yanai, Extended theoretical modeling of reverse intersystem crossing for thermally activated delayed fluorescence materials, Sci. Adv. **10**, eadk3219 (2024).

[51] T. J. Penfold, E. Gindensperger, C. Daniel, and C. M. Marian, Spin-vibronic mechanism for intersystem crossing, Chem. Rev. **118**, 6975 (2018).

[52] I. Kim, S. O. Jeon, D. Jeong, H. Choi, W. J. Son, D. Kim, Y. M. Rhee, and H. S. Lee, Spin–Vibronic model for quantitative prediction of reverse intersystem crossing rate in thermally activated delayed fluorescence systems, J. Chem. Theory Comput. **16**, 621 (2020).

[53] S. Banerjee, A. Baiardi, J. Bloino, and V. Barone, Temperature dependence of radiative and nonradiative rates from time-dependent correlation function methods, J. Chem. Theory Comput. **12**, 774 (2016).

[54] M. Etinski, J. Tatchen, and C. M. Marian, Time-dependent approaches for the calculation of intersystem crossing rates, J. Chem. Phys. **134**, 154105 (2011).

[55] E. U. Condon, A theory of intensity distribution in band systems, Phys. Rev. **28**, 1182 (1926).

[56] E. U. Condon, Nuclear motions associated with electron transitions in diatomic molecules, Phys. Rev. **32**, 858 (1928).

[57] J. Franck and E. G. Dymond, Elementary processes of photochemical reactions, Trans. Faraday Soc. **21**, 536 (1926).

[58] G. Herzberg and E. Teller, Schwingungsstruktur der Elektronenübergänge bei mehratomigen Molekülen, Z. Phys. Chem. **21B**, 410 (1933).

[59] F. Duschinsky, Zur Deutung der Elektronenspektren mehratomiger Moleküle, Acta Physicochim. URSS **7**, 551 (1937).

[60] R. Ianconescu and E. Pollak, Photoinduced cooling of polyatomic molecules in an electronically excited state in the presence of Dushinskii rotations, J. Phys. Chem. A **108**, 7778 (2004).

[61] Y. Niu, Q. Peng, C. Deng, X. Gao, and Z. Shuai, Theory of excited state decays and optical spectra: Application to polyatomic molecules, J. Phys. Chem. A **114**, 7817 (2010).

[62] A. Baiardi, J. Bloino, and V. Barone, General time dependent approach to vibronic spectroscopy including Franck–Condon, Herzberg–Teller, and Duschinsky effects, J. Chem. Theory Comput. **9**, 4097 (2013).

[63] F. Weigend and R. Ahlrichs, Balanced basis sets of split valence, triple zeta valence and quadruple zeta valence quality for H to Rn: Design and assessment of accuracy, Phys. Chem. Chem. Phys. **7**, 3297 (2005).

[64] J. P. Perdew, K. Burke, and M. Ernzerhof, Generalized gradient approximation made simple, Phys. Rev. Lett. **77**, 3865 (1996).

[65] S. Grimme, J. Antony, S. Ehrlich, and H. Krieg, A consistent and accurate *ab initio* parametrization of density functional dispersion correction (DFT-D) for the 94 elements H-Pu, J. Chem. Phys. **132**, 154104 (2010).

[66] S. Grimme, S. Ehrlich, and L. Goerigk, Effect of the damping function in dispersion corrected density functional theory, J. Comput. Chem. **32**, 1456 (2011).

[67] H. Kruse and S. Grimme, A geometrical correction for the inter- and intra-molecular basis set superposition error in Hartree-Fock and density functional theory calculations for large systems, J. Chem. Phys. **136**, 154101 (2012).

[68] F. Neese, Efficient and accurate approximations to the molecular spin-orbit coupling operator and their use in molecular g-tensor calculations, J. Chem. Phys. **122**, 034107 (2005).

[69] S. Hirata and M. Head-Gordon, Time-dependent density functional theory within the Tamm–Dancoff approximation, Chem. Phys. Lett. **314**, 291 (1999).

[70] F. Santoro and D. Jacquemin, Going beyond the vertical approximation with time-dependent density functional theory, WIREs Comput. Mol. Sci. **6**, 460 (2016).